

Assessing the accuracy of the GENIE event generator with electron scattering data: Reduced cross section and nuclear transparency

A. V. Butkevich and S. V. Luchuk

*Institute for Nuclear Research,
Russian Academy of Sciences,
Moscow 117312, Russia*

(Dated: June 25, 2025)

The reduced cross sections of the semi-exclusive $(l, l'p)$ lepton scattering process can be identified with distorted nuclear spectral functions. Irrespective of the type of interaction the distorted spectral function is determined mainly by intrinsic properties of the target and the ejected nucleon interaction with residual nucleus. Thus the reduced cross sections of the neutrino and electron scattering on nuclei as functions of nucleon missing momentum and energy are similar up to Coulomb corrections. Here we demonstrate the utility of this approach by benchmarking the GENIE neutrino event generator against a broad set of semi-exclusive electron scattering data for carbon target. We observe persistent disagreements between the generator predictions and data in the range of nucleon missing momenta less than 80 MeV/c. The approach presented in this paper provide a great opportunity to test better the accuracy of nuclear models of quasi-elastic neutrino-nucleus scattering, employed in neutrino event generators.

PACS numbers: 25.30.-c, 25.30.Bf, 25.30.Pt, 13.15.+g

I. INTRODUCTION

The primary physics goal for current [1, 2] and future [3–5] accelerator-based neutrino experiments are measuring the lepton CP violation phase, determining neutrino mass ordering, and testing the three-flavor paradigm. In these experiments to evaluate the oscillation parameters, the probabilities of neutrino oscillations as functions of neutrino energy are measured. The accuracy to which neutrino oscillation parameters can be extracted depends on the ability of experiments to determine the individual energy of detected neutrino.

The neutrino beams are not monoenergetic and have broad distributions that range from tens of MeVs to a few GeVs. At the GeV- scale neutrino energies the neutrino can interact with a nucleus through a wide range of reaction channels. These include the charged-current (CC) quasielastic (QE) scattering, two-body meson exchange current (MEC) channels, resonance production and deep inelastic scattering. The incident neutrino energy is reconstructed using kinematic or calorimetric methods. At energy about 1 GeV, where the CCQE scattering is dominant, the incoming neutrino energy can be derived from lepton kinematics alone. Conservation of total energy in neutrino interactions imply that $\epsilon_\nu = \epsilon_l + \epsilon_h$, where ϵ_ν , ϵ_l , and ϵ_h are neutrino, leptonic, and hadronic energies, respectively. The total hadronic energy deposit is obtained by summing all the visible energy not associated with lepton. A model dependent fit $\epsilon_h = f(E_{vis})$ obtained from simulation is used to relate the visible energy E_{vis} to the estimated total hadronic energy ϵ_h . Thus, the calorimetric method relies not only on the visible energy measured in the detector, but also on the models of the neutrino-nucleus interactions that are implemented in neutrino event generators. In addition the neutrino-nucleus scattering model is critical for obtaining background estimates, in analysis aimed at determining the neutrino oscillation parameters.

Unfortunately, due to wide range of neutrino energy beams and poor statistics available from current neutrino experiments, it is challenging to provide reliable and consistent predictions for the diversity of processes that can take place in the energy range covered by these neutrino beams. Various contributions to the cross sections can significantly overlap with each other making it difficult to identify, diagnose and remedy shortcomings of nuclear models. Moreover, neutrino scattering measurements are typically reported integrated over a range of energies and angles. Therefore the task to assess the accuracy of the neutrino event generators is more complicated than simply comparing generators predictions to neu-

trino data. It is necessary to come up with independent validation methods, which would allow specific physical mechanisms to be tested.

While electron and neutrino interactions are different at the primary vertex, many underlying physics processes in the nucleus are very similar. From the nuclear point of view the influence of nuclear medium effects such as the nuclear ground state and interaction of the outgoing nucleon with the residual nucleus can be expected to be largely the same for electron and for neutrino-induced processes. It is possible to exploit this similarity and use electron scattering data with precise kinematics and large statistics to test the neutrino energy reconstruction methods and interaction models.

Electron and neutrino scattering are strongly linked in theory. Therefore any model of neutrino interactions (vector+axial) should also be able to reproduce electron (vector) interactions. The vector part of the electroweak interaction can be inferred directly from the electron scattering data. A model unable to reproduce electron measurements cannot be expected to provide accurate prediction for neutrino cross sections.

Recent years have seen a plethora of analyses of electron-scattering data to test the vector current part of the lepton-nucleus interaction against existing inclusive electron scattering cross sections for different target nuclei. The relativistic distorted wave impulse approximation (RDWIA), initially designed for description of exclusive ($e, e'p$) data [6–8] and then adopted for neutrino reactions was successfully tested against inclusive (e, e') data [9, 10]. The SuSAv2 model exploits the similarities between both interaction types to guide the description of weak scattering process [11, 12]. Neutrino event generators GENIE [13–16], NuWro [17, 18], ACHILLES [19], and NEUT [50] have been extended to electron scattering and their results were compared with measured inclusive cross sections of electron-nucleus (eA) interaction.

The further progress in reducing systematic errors in neutrino oscillation experiments requires a more extensive use of measurements of final-states protons. It is needed for neutrino energy reconstruction, because more exclusive final state measurement allows to better estimate the neutrino energy and provide information about multinucleon contribution to the inclusive cross section. Inclusive reactions are relatively insensitive to the details of the final nuclear states. Therefore, rather simple models may yield inclusive and total cross sections that are not very different from cross sections calculated in the most sophisticated models, but cannot make predictions on both leptons and hadrons in the final states.

The event generators model final state interactions (FSI) of knocked-out nucleon with residual nucleon using the intranuclear cascade models. These models should be able to reproduce nuclear transparency data from electron scattering. Nuclear transparency is defined as a probability that a knocked-out nucleon leaves the residual nucleus without re-interaction. The nucleon cascade models, implemented in the GENIE [21] and NuWro [22] event generators were tested against the nuclear transparency data. It was shown that these generators are able to reproduce these data if short-range nucleon-nucleon (NN) correlations in the ground state of the nucleus are taken into account.

The semi-exclusive $(l, l'p)$ lepton scattering process involves the specific asymptotic states and allows to test more in detail the nuclear model. The reduced cross section, obtained from the measured differential semi-exclusive electron scattering cross section dividing by the kinematic factor and the off-shell electron-proton cross section, can be identified as the distorted spectral function. Thus, irrespective of the type of interaction (electromagnetic or weak) the distorted spectral function is determined mainly by the intrinsic properties of the target and the ejected nucleon interaction with residual nucleus and depends upon the initial and ejectile nucleon's momenta and angle between them. Microscopic and unfactorized RDWIA was used [23–26] for calculation of the charged-current (CC) quasielastic (QE) neutrino scattering reduced cross sections as function of the missing nucleon momentum. The results were compared with ones obtained from measurements of $(e, e'p)$ scattering on oxygen, carbon, calcium, and argon targets. It was shown, that these cross sections are similar to those of electron scattering data and are in agreement with electron scattering data. This approach provides novel constraints on nuclear models of the CCQE scattering and can be applied to test spectral functions and FSI employed in neutrino event generators.

The goal of the present paper is to carry out a systematic comparison of the CCQE reduced cross sections and nuclear transparency calculated within the models employed in the GENIE event generator [27, 28] with ones measured in electron scattering on carbon targets. For carbon targets there are high-precision data sets with different monochromatic electron energies and scattering angles. We consider GENIE because this generator is at present employed by all Femilab-based neutrino experiments.

This paper is organized as follows. In Sec.II we present briefly the formalism needed to describe the semi-exclusive lepton-nucleus CCQE scattering process. Reduced cross sections and nuclear transparency are defined. Calculations of the reduced cross sections and nuclear

transparency with neutrino event generator are described in Sec.III. In Sec.IV we regard the comprehensive model configurations employed in the GENIE v.3 simulation framework. Results and discussion of the calculations are presented in Sec.IV. Our conclusions are summarized in Sec.V.

II. FORMALISM OF QUASI-ELASTIC SCATTERING: REDUCED CROSS SECTION AND NUCLEAR TRANSPARENCY

In the laboratory frame the differential cross section for exclusive electron (σ^{el}) and (anti)neutrino (σ^{cc}) CC scattering can be written as

$$\frac{d^6\sigma^{el}}{d\varepsilon_f d\Omega_f d\varepsilon_x d\Omega_x} = \frac{|\mathbf{p}_x| \varepsilon_x \varepsilon_f \alpha^2}{(2\pi)^3 \varepsilon_i Q^4} L_{\mu\nu}^{(el)} \mathcal{W}^{\mu\nu(el)} \quad (1a)$$

$$\frac{d^6\sigma^{cc}}{d\varepsilon_f d\Omega_f d\varepsilon_x d\Omega_x} = \frac{|\mathbf{p}_x| \varepsilon_x |\mathbf{k}_f| G^2 \cos^2 \theta_c}{(2\pi)^5 \varepsilon_i 2} L_{\mu\nu}^{(cc)} \mathcal{W}^{\mu\nu(cc)}, \quad (1b)$$

where $k_i = (\varepsilon_i, \mathbf{k}_i)$ and $k_f = (\varepsilon_f, \mathbf{k}_f)$ are initial and final lepton momenta, $p_A = (\varepsilon_A, \mathbf{p}_A)$, and $p_B = (\varepsilon_B, \mathbf{p}_B)$ are the initial and final target momenta, $p_x = (\varepsilon_x, \mathbf{p}_x)$ is the ejectile nucleon momentum, $q = (\omega, \mathbf{q})$ is the momentum transfer carried by the virtual photon (W-boson), and $Q^2 = -q^2 = \mathbf{q}^2 - \omega^2$ is the photon (W-boson) virtuality. In Eqs. (1a,1b) Ω_f is the solid angle for the lepton momentum, Ω_x is the solid angle for the ejectile nucleon momentum, $\alpha \simeq 1/137$ is the fine-structure constant, $G \simeq 1.16639 \times 10^{-11} \text{ MeV}^{-2}$ is the Fermi constant, θ_C is the Cabbibo angle ($\cos \theta_C \approx 0.9749$), $L^{\mu\nu}$ is the lepton tensor, and $\mathcal{W}_{\mu\nu}^{(el)}$ and $\mathcal{W}_{\mu\nu}^{(cc)}$ are correspondingly the electromagnetic and weak CC nuclear tensors.

For exclusive reactions in which only a single discrete state or a narrow resonance of the target is excited, it is possible to integrate over the peak in missing energy and obtain a fivefold differential cross section of the form

$$\frac{d^5\sigma^{el}}{d\varepsilon_f d\Omega_f d\Omega_x} = R \frac{|\mathbf{p}_x| \tilde{\varepsilon}_x \varepsilon_f \alpha^2}{(2\pi)^3 \varepsilon_i Q^4} L_{\mu\nu}^{(el)} \mathcal{W}^{\mu\nu(el)} \quad (2a)$$

$$\frac{d^5\sigma^{cc}}{d\varepsilon_f d\Omega_f d\Omega_x} = R \frac{|\mathbf{p}_x| \tilde{\varepsilon}_x |\mathbf{k}_f| G^2 \cos^2 \theta_c}{(2\pi)^5 \varepsilon_i 2} L_{\mu\nu}^{(cc)} \mathcal{W}^{\mu\nu(cc)}, \quad (2b)$$

where R is a recoil factor

$$R = \int d\varepsilon_x \delta(\varepsilon_x + \varepsilon_B - \omega - m_A) = \left| 1 - \frac{\tilde{\varepsilon}_x \mathbf{p}_x \cdot \mathbf{p}_B}{\varepsilon_B \mathbf{p}_x \cdot \mathbf{p}_x} \right|^{-1}, \quad (3)$$

$\tilde{\varepsilon}_x$ is the solution to the equation $\varepsilon_x + \varepsilon_B - m_A - \omega = 0$, where $\varepsilon_B = \sqrt{m_B^2 + \mathbf{p}_B^2}$, $\mathbf{p}_B = \mathbf{q} - \mathbf{p}_x$ and m_A and m_B are masses of the target and recoil nucleus, respectively. Note that missing

momentum is $\mathbf{p}_m = \mathbf{p}_x - \mathbf{q}$ and missing energy ε_m are defined by $\varepsilon_m = m + m_B - m_A$. The invariant electromagnetic (weak CC) matrix element is represented by the contraction of electron (neutrino) and nuclear response tensors of the form

$$L_{\mu\nu}^{(el)(cc)} = \langle j_\mu^{(el)(cc)} j_\nu^{+(el)(cc)} \rangle \quad (4)$$

$$W_{\mu\nu}^{(el)(cc)} = \langle J_\mu^{(el)(cc)} J_\nu^{+(el)(cc)} \rangle, \quad (5)$$

where j^μ is the electron or neutrino current, $J_\mu^{(el)(cc)}$ is a matrix element of the nuclear electromagnetic or CC current, and the angled brackets denote averages over initial states and sums over final states.

The reduced cross section is given by

$$\sigma_{red} = \frac{d^5\sigma^{(el)(cc)}}{d\varepsilon_f d\Omega_f d\Omega_x} / K^{(el)(cc)} \sigma_{lN}, \quad (6)$$

where $K^{el} = Rp_x \varepsilon_x / (2\pi)^3$ and $K^{cc} = Rp_x \varepsilon_x / (2\pi)^5$ are phase-space factors for electron and neutrino scattering and

$$\sigma_{eN}^{(el)} = \frac{\varepsilon_f \alpha^2}{\varepsilon_i Q^4} (L_{\mu\nu}^{(el)} W^{\mu\nu(el)})_{PWIA} \quad (7)$$

$$\sigma_{\nu N}^{(cc)} = \frac{k_f (G_F \cos \theta_c)^2}{\varepsilon_i (2\pi)^2} (L_{\mu\nu}^{(cc)} W^{\mu\nu(cc)})_{PWIA} \quad (8)$$

are the corresponding elementary cross sections for the electron σ_{eN} and neutrino $\sigma_{\nu N}$ scattering on the moving free nucleon in the plane wave impulse approximation (PWIA) normalized to unit flux. The PWIA response tensor is computed for a free nucleon in the final state and is given by

$$W_{PWIA}^{\mu\nu} = \frac{1}{2} \text{Trace}(J^\mu J^{\nu+}), \quad (9)$$

where

$$J_{s_j, s_i}^\mu = \sqrt{\frac{m^2}{\varepsilon_i \varepsilon_j}} \bar{u}(\mathbf{p}_f, s_j) \Gamma^\mu u(\mathbf{p}_i, s_i) \quad (10)$$

is the single-nucleon current between free spinors normalized to unit flux. The initial momentum $\mathbf{p}_i = \mathbf{p}_f - \mathbf{q}_{eff}$ is obtained from the final ejectile momentum and the effective momentum transfer \mathbf{q}_{eff} in laboratory frame, and the initial energy is placed on shell. The effective momentum transfer accounts for incoming electron acceleration in the nuclear Coulomb field and $\mathbf{q}_{eff} = \mathbf{q}$ for the incoming neutrino.

The single-nucleon charged current has the $V-A$ structure $J^{\mu(cc)} = J_V^\mu + J_A^\mu$. For calculation of vertex function $\Gamma^{\mu(cc)} = \Gamma_V^\mu + \Gamma_A^\mu$ of a moving but free nucleon it is simpler to use the CC1 prescription for vector current vertex function

$$\Gamma_V^\mu = G_M(Q^2)\gamma^\mu - \frac{\bar{P}^\mu}{2m}F_M(Q^2) \quad (11)$$

and the axial current vertex function

$$\Gamma_A^\mu = F_A(Q^2)\gamma^\mu\gamma_5 + F_P(Q^2)q^\mu\gamma_5, \quad (12)$$

where $\bar{P} = (\varepsilon_f + \bar{\varepsilon}, 2\mathbf{p}_x - \mathbf{q})$ and $\bar{\varepsilon} = \sqrt{m^2 + (\mathbf{p}_x - \mathbf{q})^2}$. The weak vector form factors F_V and F_M are related to corresponding electromagnetic ones for proton $F_{i,p}^{(el)}$ and neutron $F_{i,n}^{(el)}$ by the hypothesis of conserved vector current (CVC)

$$F_i = F_{i,p}^{(el)} - F_{i,n}^{(el)} \quad (i = V, M). \quad (13)$$

For the axial F_A and pseudoscalar F_P form factors we use the dipole approximation.

The reduced cross section can be regarded as the nucleon momentum distribution modified by FSI, i.e. as the distorted spectral function. Final-state interactions make the reduced cross sections $\sigma_{red}(\mathbf{p}_m, \mathbf{p}_x)$ depend upon ejectile momentum \mathbf{p}_x , angle between the initial and final nucleon momentum and upon incident lepton energy. In the nonrelativistic PWIA limit, σ_{red} reduces to the bound-nucleon momentum distribution. These cross sections for (anti)neutrino scattering off nuclei are similar to the electron scattering apart from small differences at low beam energy due to effects of Coulomb distortion of the incoming electron wave function as shown in Refs. [23–25].

The factorization approximation to the knockout cross section stipulates that

$$\frac{d^5\sigma^{(el)(cc)}}{d\varepsilon_f d\Omega_f d\Omega_x} = K^{(el)(cc)} \times \sigma_{lN} \times \sigma_{red}(\boldsymbol{\varepsilon}_m, \mathbf{p}_m, \mathbf{p}_x). \quad (14)$$

This factorization implies that the initial nuclear state and FSI effects are decoupled from the leptonic vertex with preserved correlations between the final lepton and nucleon. In the nonrelativistic PWIA limit the fivefold differential cross section Eq.(1a) and Eq.(1b) may be expressed as product of the phase-space factor K , elementary cross section σ_{eN} , and nucleon momentum distribution $S(\mathbf{p}_m, \boldsymbol{\varepsilon}_m)$. Such factorization is not strictly valid relativistically because the binding potential alters the relationship between lower and upper components of a Dirac wave function [29].

The nuclear transparency measured as a function of Q^2 , is defined as

$$T_{exp}(Q^2) = \frac{\int_V d^3p_m d\boldsymbol{\varepsilon}_m Y_{exp}(\boldsymbol{\varepsilon}_m, \mathbf{p}_m)}{f \int_V d^3p_m d\boldsymbol{\varepsilon}_m Y_{PWIA}(\boldsymbol{\varepsilon}_m, \mathbf{p}_m)}, \quad (15)$$

where Y_{exp} and Y_{PWIA} are proton yields and theoretical calculations within the PWIA, respectively and f is a correction factor describing the depletion of the single-hole spectral function. The PWIA model describe the nuclear structure, assuming the independ particle shell model (IPSM). The calculation within the IPSM overestimate single-particle strength, because the shells are not fully occupied due to the short-range nucleon-nucleon (NN) correlations, leading to the appearance of high-energy and high-momentum components in the ground state of target. The phase space volume V is restricted to the quasielastic region by the conditions $\boldsymbol{\varepsilon}_m \leq 80$ MeV and $|\mathbf{p}_m| \leq 300$ MeV/c. One should note that measured nuclear transparency is model dependent, because it relies on the accuracy of PWIA calculations.

Similarly, a theoretical definition of nuclear transparency takes the form

$$T_{th}(Q^2) = \frac{\sum_{\alpha} \int dp_m p_m \sigma_{FSI}(\boldsymbol{\varepsilon}_{\alpha}, \mathbf{p}_m)}{\sum_{\alpha} \int dp_m p_m \sigma_{PWIA}(\boldsymbol{\varepsilon}_{\alpha}, \mathbf{p}_m)}, \quad (16)$$

where the numerator integrates the reduced cross section calculated within nuclear model, that includes the distortion due to FSI and the denominator integrates the PWIA cross section for the same model of the spectral function. In Eq. (16) sums are taken over orbits α and $\boldsymbol{\varepsilon}_{\alpha}$ is the missing energy for orbital α .

III. NEUTRINO EVENT GENERATOR AS A TOOL IN REDUCED CROSS SECTION AND TRANSPARENCY STUDIES

To test nuclear models employed in the GENIE event generator we compare reduced cross sections and nuclear transparency data for carbon nucleus with predictions made within GENIE simulation framework. The carbon nucleus which is by far most extensively studied in electron scattering experiments was used. This framework offers several models for nuclear ground state, several models for each of the eA or νA scattering mechanisms and several models for hadronic final interaction, i.e. intranuclear rescattering of the outgoing hadrons.

Only CCQE neutrino interactions with carbon nucleus were simulated. To select events and their kinematics in the stable final state which correspond to a $1\mu 1p + X$ signal, we choice events with one proton and any number of neutrons. We then make sampling of $1\mu 1p$

events from cascade model which have not been affected by inelastic FSI. Two methods are used for this. The first based on the topology of the events in the GENIE cascade, and second based solely on the knowledge of the kinematics of events Ref. [30].

For the first the GENIE output which yield for every event a number of hadrons emitted from the nucleus was used. When only one proton track is presented in an event, the original proton escapes the nucleus without inelastic interactions. When multiple tracks are present, FSI has occurred and the original proton generally change energy. On the other hand, one may want to make a selection of events based purely on the lepton and nucleon kinematics. As we are simulating, we know the true incoming energy and we can define for each event a missing energy as

$$\tilde{\epsilon}_m = \epsilon_\nu - \epsilon_\mu - T_p = \omega - T_p. \quad (17)$$

This new definition of the missing energy does not take into account explicitly the recoil energy of the residual hadronic system. In electron scattering experiments where the initial energy is known the events with $\epsilon_{min} \leq \tilde{\epsilon}_m \leq \epsilon_{max}$ are separated.

We make a selection of events, after applying the GENIE cascade, in which only those events that corresponds to the range of $\tilde{\epsilon}_m \leq 80$ MeV are present. In “perpendicular kinematics” used in electron scattering experiments Refs. [31–35] the incident energy and energy transfered are fixed, as are the electron scattering angle and the outgoing proton energy, whereas the missing momentum changes with the proton angle. It is necessary to choose the electron angle and outgoing proton energy such that $|\mathbf{p}_x| = |\mathbf{q}|$. The vectors \mathbf{p}_m and \mathbf{p}_x are almost perpendicular.

As in all electron scattering experiments the lepton and hadron spectrometers are set in plane, the out-of-plane angles are fixed to $\phi_e = 0^\circ$ and $\phi_p = 180^\circ$. The sixfold exclusive cross section is given by

$$\frac{d^6 \sigma}{d\epsilon_\mu d\Omega_\mu dT_p d\Omega_p} = \frac{N_{1\mu 1p}}{N_{tot}} \frac{\sigma_{tot}(\epsilon_\nu)}{\Delta\epsilon_\mu \Delta T_p \Delta\Omega_\mu \Delta\Omega_p}, \quad (18)$$

where N_{tot} is the total number of generated CCQE neutrino events with a total CCQE cross section $\sigma_{tot}(\epsilon_\nu)$ at energy ϵ_ν . $N_{1\mu 1p}$ is the number of selected $1\mu 1p$ events in the differential phase space volume bin $\Delta V = \Delta\epsilon_\mu \Delta T_p \Delta\Omega_\mu \Delta\Omega_p$ with the central values $\epsilon_\mu, T_p, \Omega_\mu, \Omega_p$ and with size of differential bins $\Delta\epsilon_\mu, \Delta T_p, \Delta\theta_\mu, \Delta\theta_p, \Delta\phi_\mu, \Delta\phi_p$. The central values and size of the differential bins of kinematic variables are given in Table I and Table II, corresponding, for every data set that is analyzed in this work. To go from measured variables ϵ_μ and T_p

data set	ε_i (MeV)	ε_f (MeV)	θ_e (deg)	T_p (MeV)	θ_p (deg)	$\Delta\varepsilon_m$ (MeV)	Q^2 (GeV ²)
Tokyo [31, 32]	700	525	52.3	156	49.7 - 70.2	80	0.29
Saclay [33]	497	375	52.9	87	48 - 91	60	0.16
SLAC [34]	2015	1390	35.5	600	43.4 - 54.6	80	1.11
JLab [35]	2445	2075	20.5	350	35.4 - 75.4	80	0.64

TABLE I. Summary of data for $^{12}\text{C}(e, e'p)$. ε_i is the beam energy, ε_f is the central electron energy, θ_e is the central electron angle, T_p is the central proton kinetic energy, θ_p is the central proton angle, $\Delta\varepsilon_m$ is the range of the missing energy.

data set	$\Delta\varepsilon_f$ (%)	$\Delta\theta_e$ (deg)	ΔT_p (%)	$\Delta\theta_p$ (deg)	$\Delta\phi_e$ (deg)	$\Delta\phi_p$ (deg)
Tokyo [31, 32]	9.5	5	38	3	3	3
Saclay [33]	18	2	23	2	6	6
SLAC [34]	4	3	8	1	3	3
JLab [35]	4	1.5	14	1	3	3

TABLE II. Table of the experimental cuts that used in simulation. $\Delta\varepsilon_f$ is the electron energy acceptance, $\Delta\theta_e$ is the electron angle acceptance, ΔT_p is the proton kinetic energy acceptance, and $\Delta\phi_p$ is the proton angle acceptance, $\Delta\phi_e$ is the electron plane angle acceptance.

to

$$\varepsilon_m = \omega - T_p - \varepsilon_B \quad (19)$$

and

$$p_m = [p_x^2 + k_\nu^2 + k_\mu^2 - 2k_\mu k_\nu \cos \theta_\mu - 2p_x k_\nu \cos \theta_p + 2k_\mu p_x \cos \theta_{\mu p}]^{1/2} \quad (20)$$

we use the formula

$$\frac{d^6\sigma}{dp_m d\varepsilon_m d\Omega_\mu d\Omega_p} = \frac{d^6\sigma}{d\varepsilon_\mu dT_p d\Omega_\mu d\Omega_p} / J(\theta_p), \quad (21)$$

where Jacobin $J = \partial(\varepsilon_m, p_m) / \partial(\varepsilon_\mu, T_p)$ is equal to

$$J(\theta_p) = \frac{1}{p_m} (k_\mu - k_\nu \cos \theta_\mu + p_x \cos \theta_{\mu p}) - \frac{\varepsilon_x}{2p_m} \frac{p_x^2 + p_m^2 - |\mathbf{q}|^2}{p_x^2}. \quad (22)$$

In Eq.(21) $\cos\theta_{\mu p} = \cos(\theta_\mu + \theta_p)$ and we assess positive (negative) values to p_m for the condition $\theta_p < \theta_q$ ($\theta_p > \theta_q$), where $\cos\theta_q = \mathbf{p}_x \cdot \mathbf{q}/(|\mathbf{p}_x||\mathbf{q}|)$. Then we can determine

$$\frac{d^2\sigma}{dp_m d\epsilon_m} = \frac{d^6\sigma}{dp_m d\epsilon_m d\Omega_\mu d\Omega_p}, \quad (23)$$

as a function of missing energy and missing nucleon momentum. All nuclear models which implemented in the GENIE generator do not allow calculation of the $d^2\sigma/dp_m d\epsilon_m$ distribution as function of ϵ_m , as well as the calculation of the $d\sigma/dp_m$ in ranges $10 < \epsilon_m < 25$ MeV ($1p_{3/2}$ shell) and $30 < \epsilon_m < 50$ MeV ($1s_{1/2}$ shell), because they use one-dimensional $d\sigma/dp_m$ distributions with fixed values of binding energy. Therefore we can evaluate only the $d\sigma/dp_m$ cross section

$$\frac{d\sigma}{dp_m} = \Delta\epsilon_m \frac{d^2\sigma}{dp_m d\epsilon_m} \quad (24)$$

as a function of p_m , integrated over range $\Delta\epsilon_m$, that is given in Table I. Then the reduced cross section can be written as

$$\sigma^{red}(p_m) = \frac{1}{K\sigma_{\nu N}} \frac{d\sigma}{dp_m}(p_m). \quad (25)$$

The calculation of $\sigma_{\nu N}$ is performed with the same nucleon form factors as GENIE σ/dp_m cross section calculation.

The experimental definition of the nuclear transparency Eq.(15), which is given by ratio of the observed number of $1\mu 1p$ events (without FSI) to the ones predicted in the PWIA as a function of T_p was used. We take into account a finite energy acceptance $\Delta T_p/T_p \approx 0.2$ of hadronic spectrometers.

IV. COMPREHENSIVE MODEL CONFIGURATIONS IN GENIE FRAMEWORK

As mentioned above, the GENIE v3 simulation framework uses a few different models of nucleon momentum distribution in the nuclear ground state. It also offers several models of quasielastic lepton-nucleus interactions and several intranuclear cascade models for FSI.

We use the GENIE Version 3.04.00 and consider five distinct sets of GENIEs models for CCQE scattering namely: the G18-02a (RFG), G18-10a (LFG), G21-11a (SuSAv2-MEC), sf1d (SF), and effsf (effective spectral function) models Refs [36–38]. These models are accompanied by the FSI models available in the GENIE [36]. The effective intranuclear

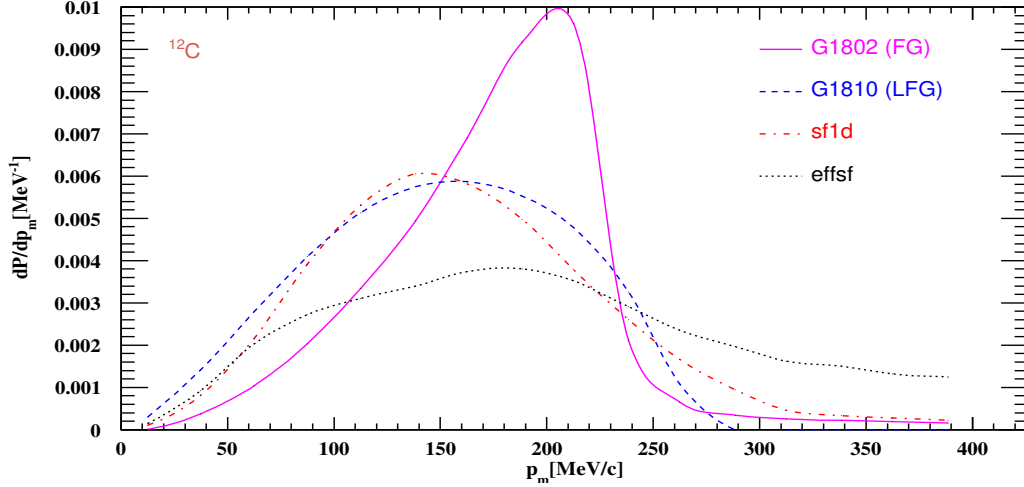


FIG. 1. Initial nucleon momentum distribution for ^{12}C according to GENIE implementation of G18_02a (FG, solid line), G18_10a (LFG, dashed line), sf1d (dashed-dotted), and effsf (dotted line) models.

model INTRANUKE hA is an empirical data driven method, uses the cross sections of pions and nucleons interactions with nuclei as a function of energy up to 1.2 GeV. For higher energies the GEM03 calculation [39], normalized to low energy data is used. The INTRANUKE hN model is a full intranuclear cascade calculation of pion, kaon, photon, and nucleons interactions with nuclei up to 1.2 GeV.

The G18_02a configuration of GENIE used for CCQE interaction on nuclei relies on implementation of the relativistic Fermi gas model (RFG) which has been modified to incorporate short-range NN-correlations [40]. For quasielastic and elastic scattering, Pauli blocking is applied and CCQE scattering is simulated by the Llewellyn-Smith model [41]. The G18_10a model set includes the full Valencia model [42–44] for the local Fermi gas (LFG) nucleon momentum distribution. It also uses the random phase approximation (RPA) which is a description of long-range and short-range NN-correlations. The main effect of the RPA corrections is a suppression of the CCQE cross section at low Q^2 . The G21_11 model, based on the SuSAv2 approach uses superscaling to write the inclusive CCQE cross section in terms of a universal function [45]. The superscaling phenomenon is shown by electron-nucleus scattering data. The nucleon kinematics in this model are determined by choosing its initial momentum from the LFG distribution.

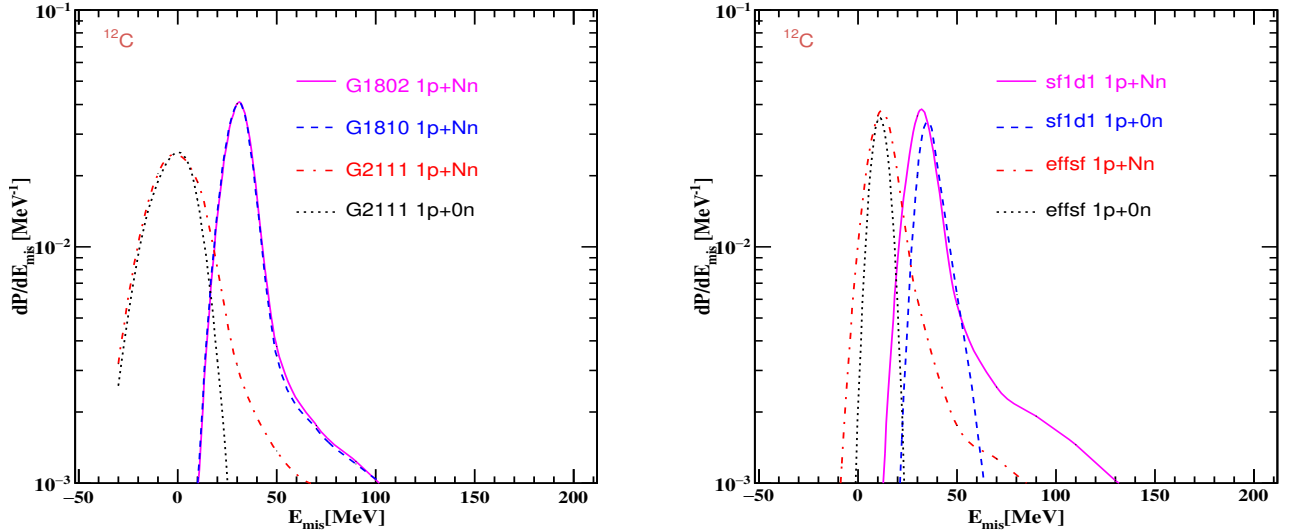


FIG. 2. Probability density distribution vs missing energy E_{mis} calculated for neutrino energy $\varepsilon_\nu = 0.5$ GeV. Left panel: PDF for (1p+Nn) events calculated with the G18_02 (solid line), G18_10 (dashed line), G21_11 (dashed-dotted line) models and for (1p+0n) events calculated within G21_11 (dotted line) model. Right panel: PDF for (1p+0n) set calculated with sf1d (solid line), effsh (dotted line) model and PDF for (1p+Nn) set calculated within the sf1d (dashed line) and effsf (dashed-dotted line) models.

The sf1d model that is included in GENIE simulation framework as an option Spectral-Function1d is based on spectral functions (SF) for finite nuclei derived from correlated basis function approach [46, 47]. The SF is a sum of mean field and correlation terms with distinct energy and momentum distribution. The mean field piece has been fitted to the (e,e'p) scattering data and the correlation contribution is computed using the local density approximation. The spectral function for proton and neutron are the same. The effective spectral function (effsf) model with or without enhancement contribution [48, 49] is implemented in the GENIE as an option EffectiveSF. In this model the magnetic form factor for bound nucleon is modified to describe the enhancement of transverse contribution in the quasielastic cross section of electron-carbon scattering. In this work all five models are accompanied by the FSI using the effective intranuclear cascade model INTRANUKE hA.

Figure 1 displays the bound nucleon momentum distribution in carbon for the genuine

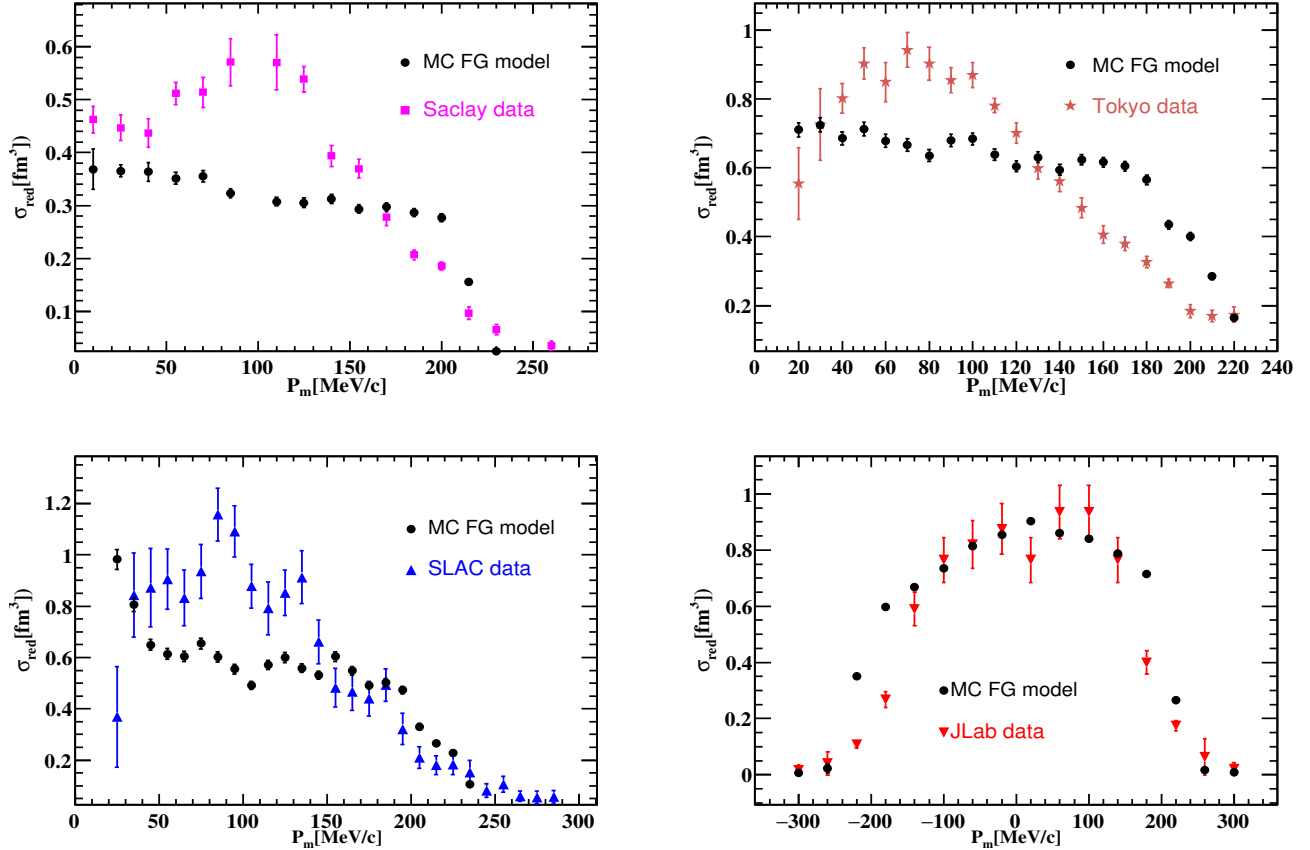


FIG. 3. Comparison of the GENIE G18_02a (FG model) calculation reduced cross sections with data as function of missing momentum. As shown in the key, cross sections were calculated for Saclay [33], Tokyo [31, 32], SLAC [34], and JLab [35] kinematics.

CCQE events produced using the GENIE and the RFG, LFG, sf1d and effs representations of the target nucleus. It is clearly visible that the probability density function (PDF) dP/dp_m calculated with the RFG in the range $150 \leq p_m \leq 220$ ($p_m \leq 50$) (MeV/c) is much larger (smaller) than PDFs used in the other models, plus correlation tails are observed in the RFG, sf1d, and effs distributions. As mentioned before, we consider two sets of events in which the neutrino knocks out a proton. The first set contains events with a muon and only one proton ($1p + 0n$) in the final state. Such events are selected in electron scattering experiments ($e, e'p$) to measure reduced cross sections. The second set contains events with a muon, one proton, and at least one neutron ($1p + Nn$) in the final state. In neutrino experiments these two sets of events are not distinguished, because the incident neutrino

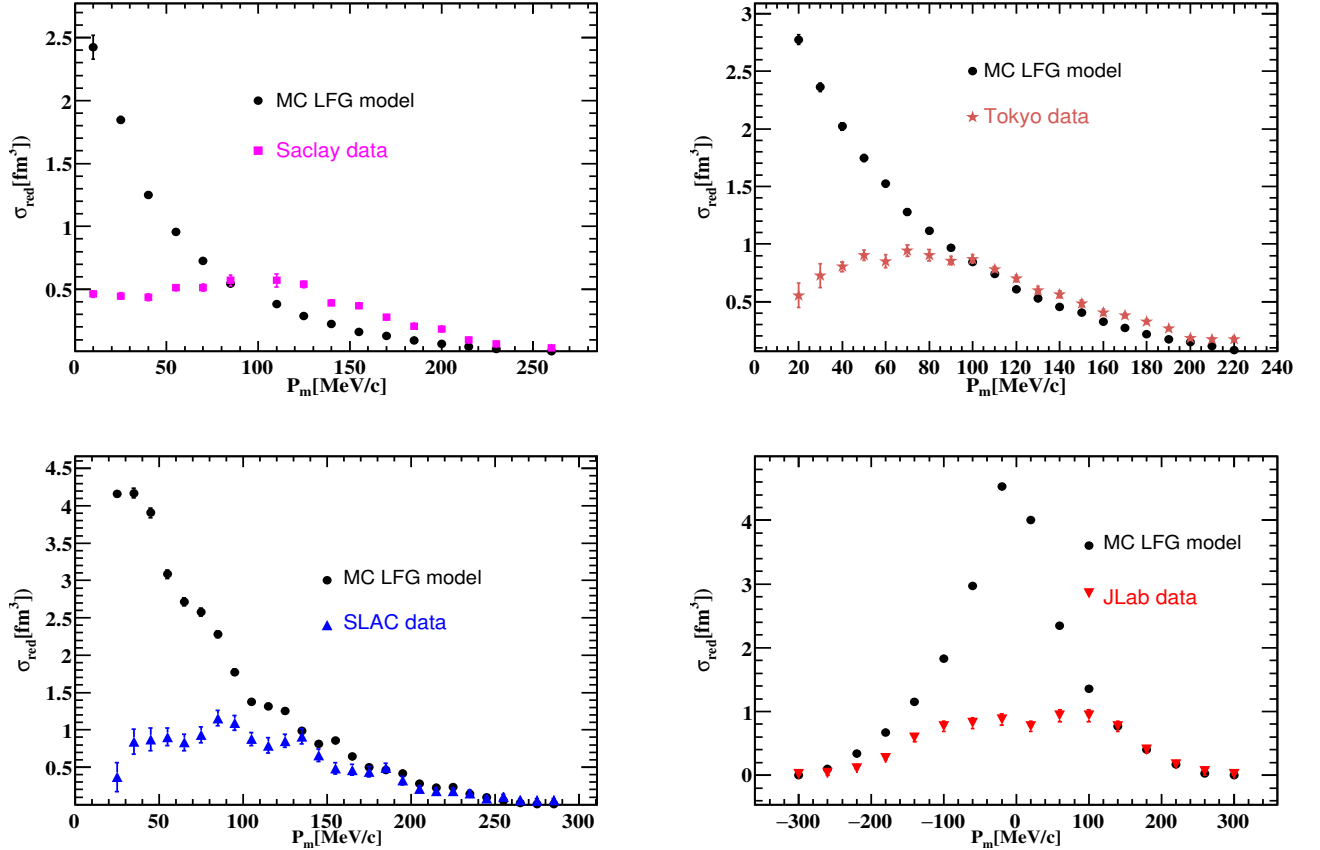


FIG. 4. Same as Fig. 3 but for the G18_10a (LFG) model calculation.

energy is unknown. The missing energy $E_{mis} = \varepsilon_\nu - \varepsilon_\mu - T_p$ distributions for (1p+0n) and (1p+Nn) ($N \leq 3$) sets calculated for neutrino energy $\varepsilon_\nu \leq 0.5$ GeV using five GENIE' models are shown in Fig. 2. For all models (except G21_11 model) maximum of distribution is located in the range $E_m \leq 40$ MeV. For the G18_02a and G18_10a models the distributions of events in (1p+0n) set have narrow peak in the range $20 \leq E_m \leq 40$ MeV. The inelastic scattering changes the energy of the knocked out protons significantly and therefore the distributions of events in the (1p+Nn) set are continued into higher missing region.

V. RESULTS AND ANALYSIS

For each model considered we generated 10^8 CCQE neutrino events. The reduced cross sections calculated with the GENIE G18_02a model that uses the RFG nucleon momentum

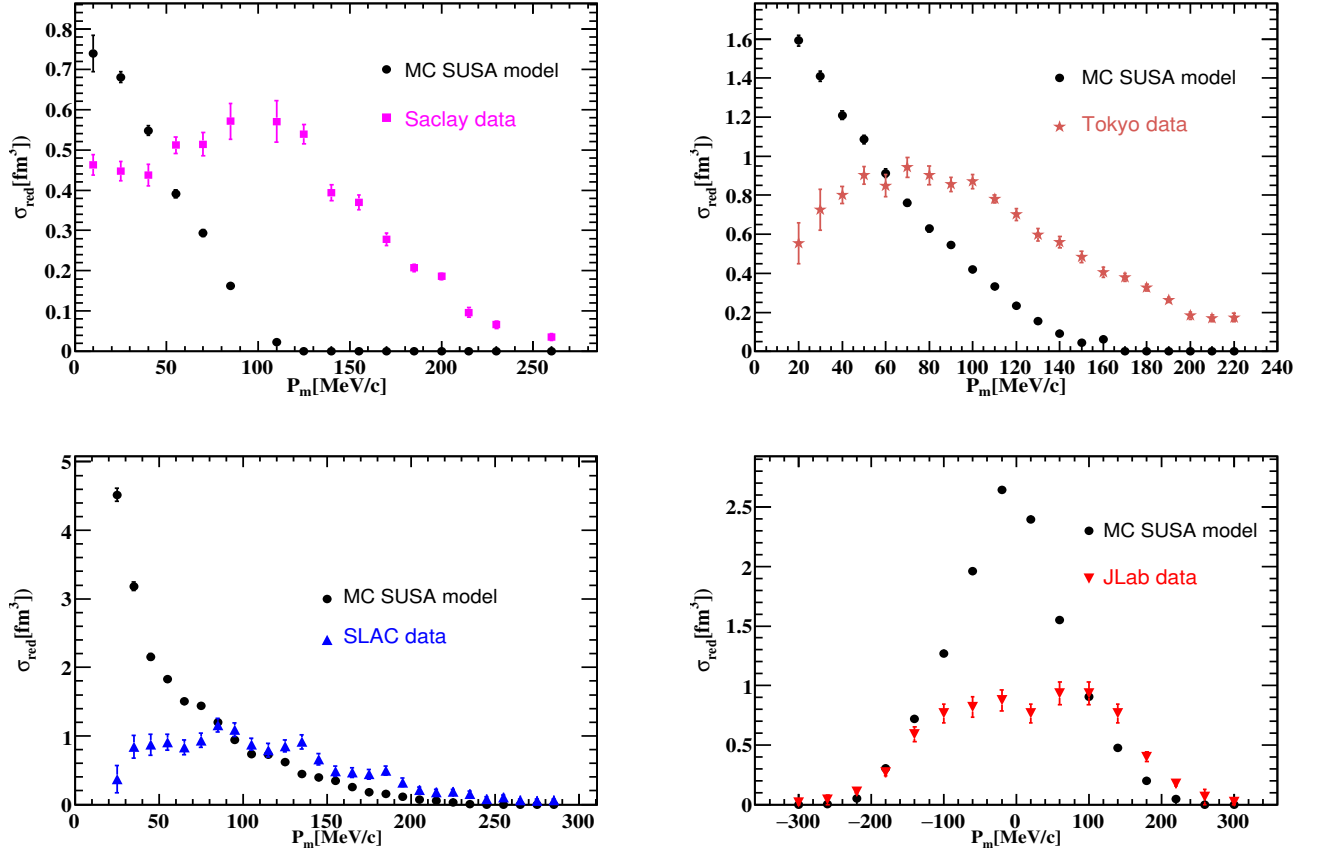


FIG. 5. Same as Fig. 3 but for the G21_11 (SUSAv2) model calculation.

distribution are shown in Fig. 3 together with Saclay [33], Tokyo [31, 32], SLAC [34], and JLab [35] data. It should be noted that negative values of p_m corresponds to $\phi = \pi$ and positive ones to $\phi = 0$. The cross sections were calculated using the kinematic conditions of data examined that is presented in Tables I and II. The values of measured cross sections at the maximum are higher than calculated ones with exception for JLab kinematics. Discrepancies up to 50% at the maximum are observed with low beam energy (low Q^2) for Saclay and Tokyo data and they decrease with the increasing the beam energy. There is an overall agreement with JLab data at $E_\nu = 2.4$ GeV. The difference between the electron and neutrino reduced cross sections about 10% can be attributed to Coulomb distortion upon electron wave function. The electron effective momentum is larger than the value of electron momentum at infinity, because of Coulomb attraction. The flux is also increased in the interaction zone by the focusing of the electron wave. This effect weakens as the beam energy

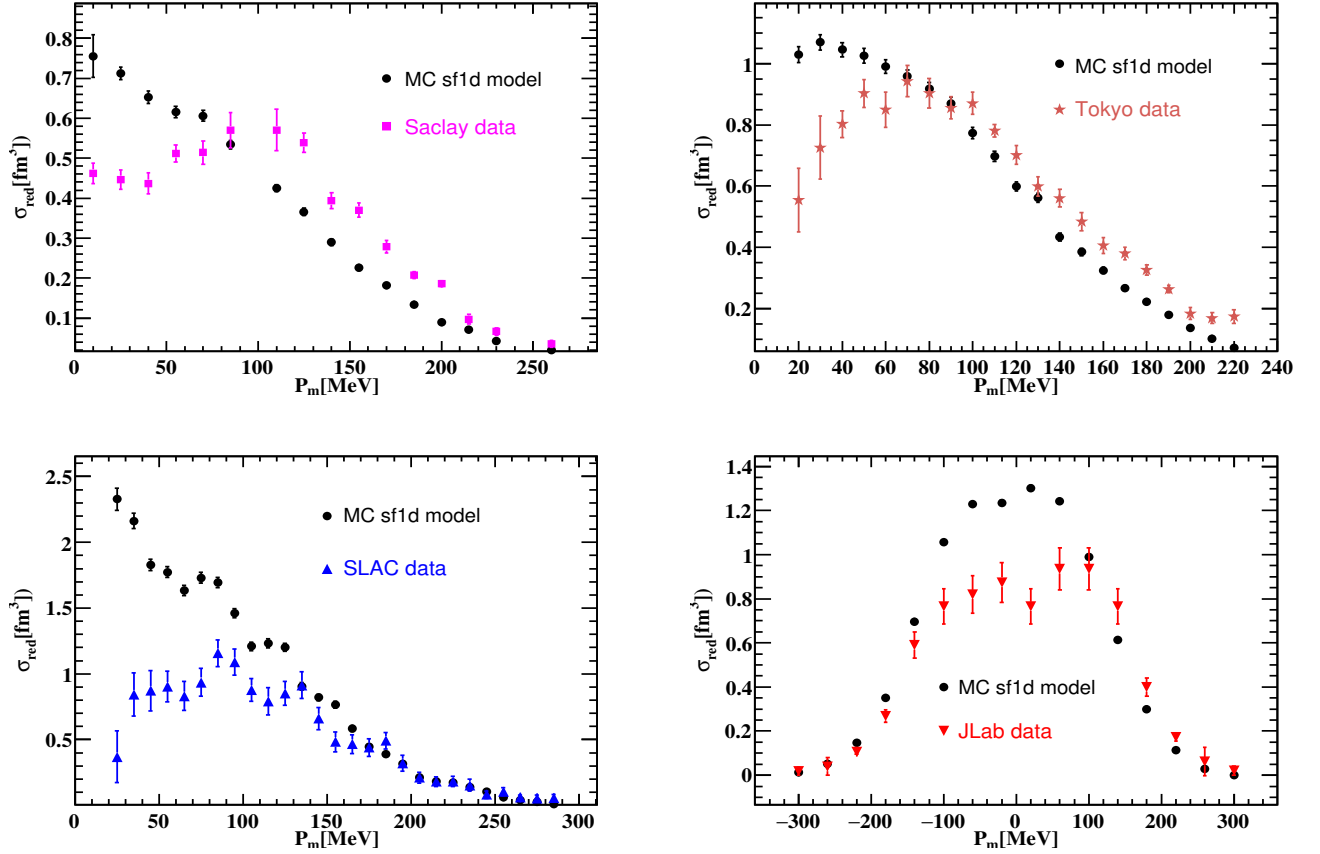


FIG. 6. Same as Fig. 3 but for the sf1d (SF) model calculation.

increases, and for this reason this effect is more significant at Saclay and Tokyo kinematics ($\epsilon_\nu = 500$ MeV) than at JLab kinematics ($\epsilon_\nu = 2.5$ GeV).

The reduced cross section for removing a nucleon in $^{12}\text{C}(\nu_\mu, \mu p)$ reaction, calculated with the GENIE G18.10a model, is shown in Fig. 4 as a function of missing momentum together with data. This model uses the LFG nucleon momentum distribution taking into account the RPA corrections. At $|p_m| \leq 50$ MeV/c the calculated cross sections are significantly higher than measured ones. The range $|p_m| \leq 100$ MeV/c corresponds to the proton scattering angles $43^\circ \leq \theta_p \leq 63^\circ$. The difference decreases as the p_m increases. In the range $|p_m| \geq 100$ MeV/c there is an overall agreement between calculated and measured reduced cross sections.

Figure 5 shows the same as Fig. 3 but for reduced cross sections calculated within the G21.11 model, where LFG nucleon momentum distribution is used as well. The σ_{red} calcu-

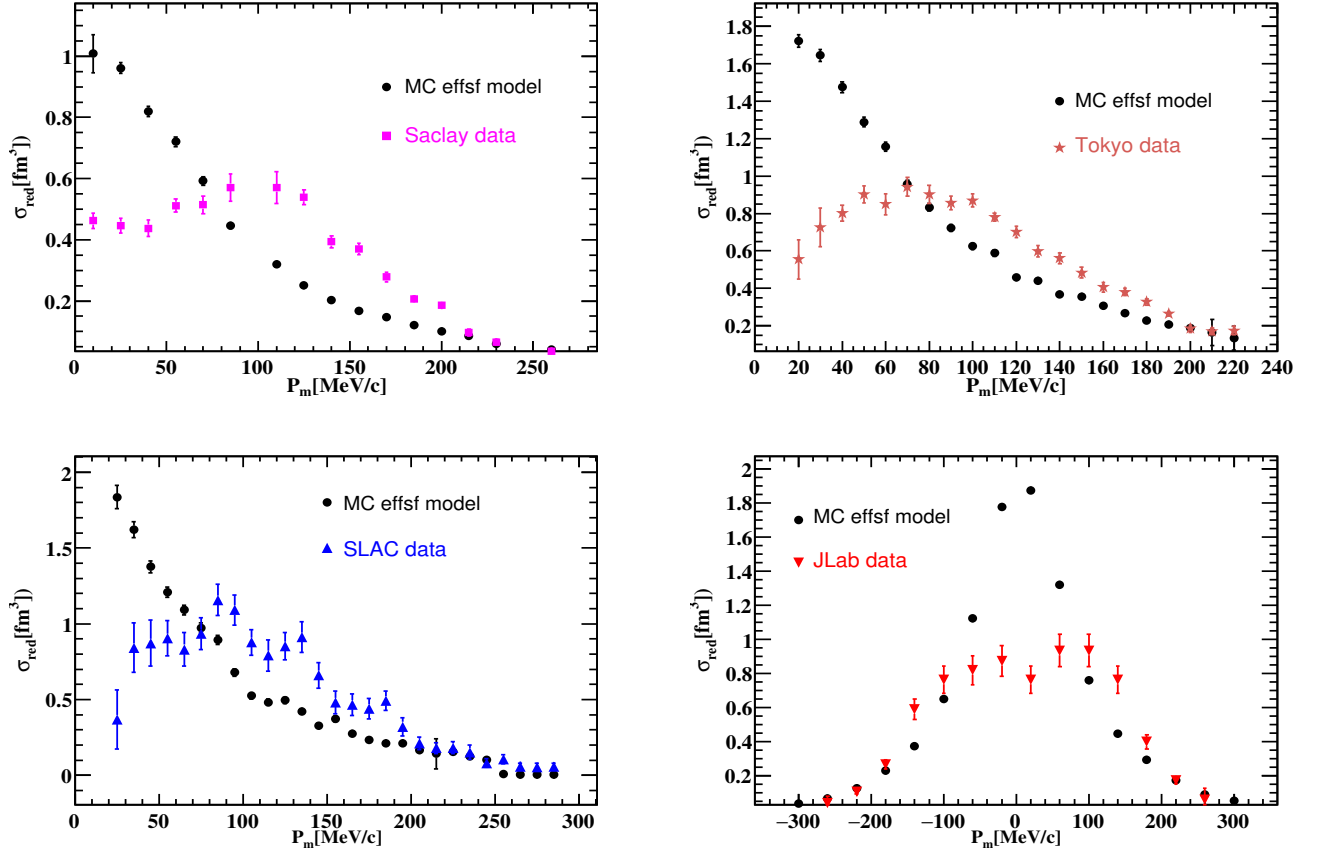


FIG. 7. Same as Fig. 3 but for the sf1d (SF) model calculation.

lated with this model for Saclay [33] and Tokyo [31, 32] kinematics demonstrate absolutely different behavior than measured ones. At the SLAC [34] and JLab [35] kinematics the issues visible at momenta less than 100 MeV/c resemble those for the G18_10a model seen in Fig. 4.

In Fig. 6 we compare the GENIE sf1d model calculations with the data for reduced cross sections of electron scattering on carbon. It's obvious that the calculated σ_{red} at $p_m \leq 50$ MeV/c overestimate the measured ones. The excess increases with the decrease of missing momentum and reaches up to 50-60% and higher for the SLAC kinematics. At $p_m \geq 50$ MeV/c the measured cross sections are lower than calculated σ_{red} and discrepancy reduces with the beam energy (Q^2). The calculations are in a good agreement with SLAC and JLab data in the region $p_m \geq 100$ MeV/c. Approximately the same features are observed in Fig. 7 where the comparison with data of the reduced cross sections calculated with the GENIE

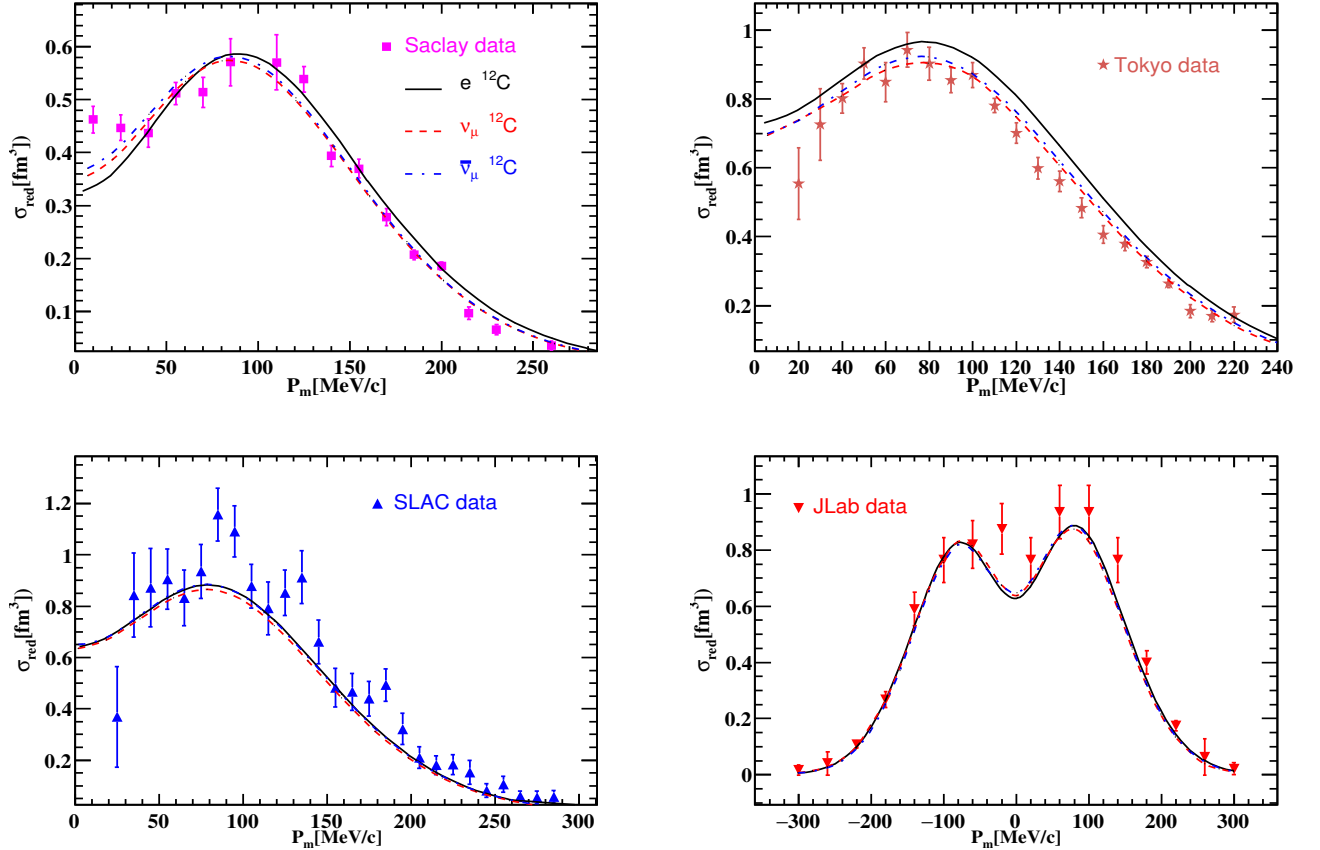


FIG. 8. Same as Fig. 3 but for the RDWIA model calculation.

effsf model is presented. The calculated cross sections overestimate the measured ones at $p_m \leq 80$ MeV/c and underestimate data at higher missing momentum.

So, we observe persistent disagreement between the GENIE predictions of the reduced cross sections and electron scattering data at low beam energy and Q^2 . For the models considered (except the RFG model) the issues are similar: the calculations overestimate data significantly at low missing momenta and underestimate gently at $p_m \geq 100$ MeV/c. For example, the best values of $\chi^2/DOF \approx 12.6$ are observed for the effsf model calculation and SLAC data, and $\chi^2/DOF \approx 17.5$ for the sf1d model prediction and JLab data.

The reduced cross sections calculated in Refs. [24–26] within the relativistic distorted wave impulse approximation (RDWIA) with the EDAD1 parametrization of the optical potential are shown in Fig. 8 together with Saclay [33], Tokyo [31, 32], SLAC [34], and JLab [35] data. The cross sections were calculated for electron and (anti)neutrino scattering on carbon.

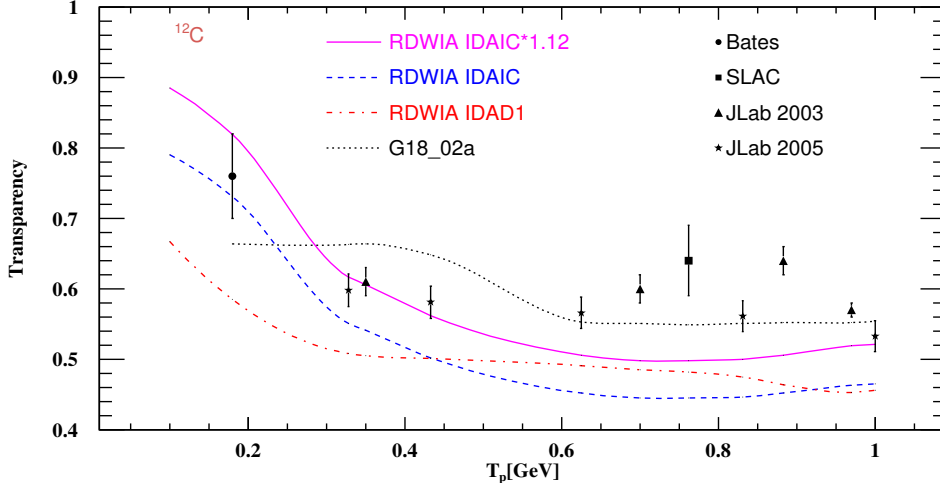


FIG. 9. Nuclear transparency as a function of proton kinetic energy. Calculations compared with measured nuclear transparency data of Bates [51], SLAC [34], JLab 2003 [35], and JLab 2005 [52] experiments. As shown in the key nuclear transparencies were calculated in the RDWIA with the IDAIC, IDAD1 optical potentials, and with GENIE G18_02a model.

There is a good agreement between the RDWIA calculated and measured cross sections. So, microscopic and unfactorized model like the RDWIA can be used to model both lepton-boson and boson-nucleus vertexes [50]. Apparently, this model describes better the semiexclusive ($l, l'p$) lepton scattering process than the phenomenological models employed in the GENIE simulation framework. In Fig. 9 the GENIE G18_02a nuclear transparency result for carbon is shown with data for $^{12}\text{C}(e, e'p)$ from Bates [51], SLAC [34], and JLab [35, 52]. The transparency curve has a characteristic shape: a saturation at larger values of proton kinetic energy and decline in the region of 1 GeV. Saturation can be explained by a roughly constant value of the total nucleon-nucleon cross sections for larger values of the incident nucleon momentum. This simulation slightly underestimates data in the saturation region, but in general the agreement with data is satisfactory.

Also shown in Fig. 9 are the results obtained by Kelly in the RDWIA using several parametrizations of the optical potential [32]. All of these calculations systematically underestimate the experimental transparency. Multiplying the EDAIC results by 1.12 provides a reasonable description of the data over this range of ejectile energies. The author concluded that a more detailed model of the continuum arising from multinucleon knockout that

contribute approximately 12% of strength for $\epsilon_m \leq 80$ MeV is needed.

Comparison of the EDADIC result multiplied by 1.12 and result of the calculation with the G18_10a model performed in this work is shown in Fig. 10 on the left panel. Also shown are the results obtained in Ref. [21] with the GENIE G18_10a model (GENIE hA2018) and in Ref. [22] using the NuWro neutrino event generator. The results obtained within the G18_10a in this work and in Ref. [21] are in good agreement. On the other hand the values of the NuWro nuclear transparency are systematically larger than those obtained in our calculation. In Fig. 10 on the right panel the nuclear attenuations calculated within the RDWIA for the individual shells in ^{12}C are presented. The calculations were performed with the EDAD1 and EDAIC approximations of the optical potential. Investigating the attenuation for each individual shell allow one to study the radial dependence of the FSI mechanisms. In the ^{12}C case, for example, the $1s_{1/2}$ orbit has spatial characteristics which are very different from the $1p_{3/2}$ orbit. As expected, the RDWIA model predict a stronger attenuation for proton emission from a level which has a larger fraction of its density in the nuclear interior.

VI. CONCLUSIONS

In this paper we show that reduced cross sections and nuclear transparencies measured in QE electron-scattering experiments can serve as a very effective tool for testing neutrino event generators. This is made possible by two factors. First these experiments features precisely known electron and proton kinematics: initial electron energy and energies of the scattered electron and proton as well as their scattering angles. Second there are numerous (at least for carbon) electron-scattering reduced cross section datasets covering the range of energies and angles relevant to neutrino oscillation experiments. We carried out a systematic comparison of the CCQE reduced cross sections and nuclear transparency calculated with the models employed in the GENIE v3 simulation framework with the data measured in electron scattering off carbon target. Because these data have not been previously used to tune the parameters of the neutrino events generators they present great opportunity to test the accuracy of the cross section estimates.

We have observed persistent disagreements between the GENIE predictions and electron scattering data for reduced cross sections. Below missing momentum $p_m \approx 80$ MeV/c the

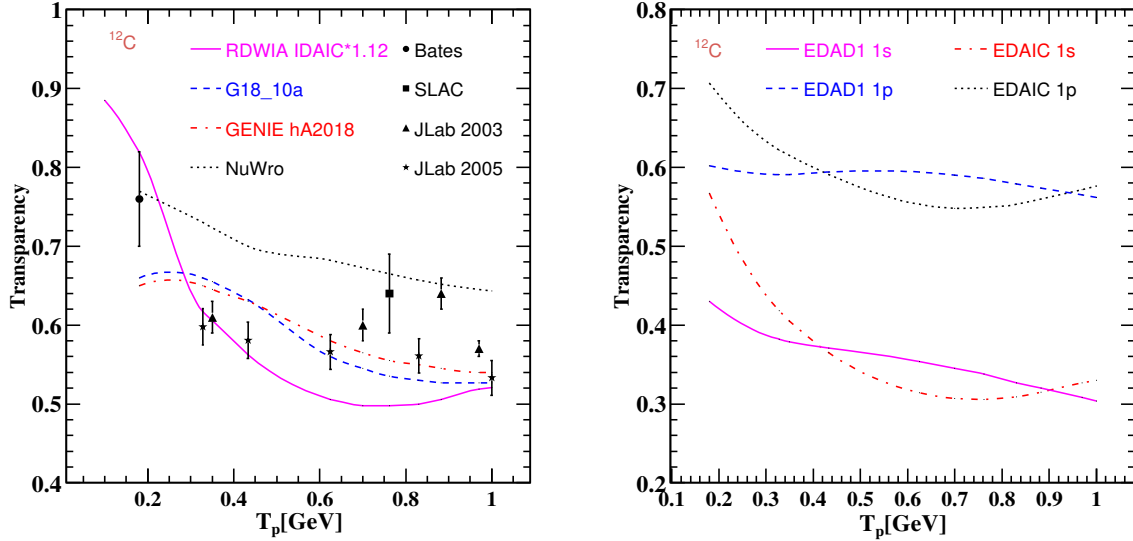


FIG. 10. Nuclear transparency as a function of proton kinetic energy. Left panel: the RDWIA calculation with the IDAIC optical potential, G18_10a model and NuWro generator results compared with measured nuclear transparency data of Bates [51], SLAC [34], JLab 2003 [35], and JLab 2005 [52] experiments. Right panel: transparency for the $1p_{3/2}$ and $1p_{1/2}$ orbits in ^{12}C as obtained in the RDWIA with the IDAIC and IDAD1 optical potentials.

reduced cross sections predicted by the GENIE models based on the LFG nucleon momentum distribution (G18_10a and G21_11 models) overestimate data significantly. On the other hand apparently that microscopic and unfactorized model like the RDWIA describes the semiexclusive lepton scattering reactions better than the phenomenological models employed in the GENIE generator.

The study of the nuclear transparency presented in this paper showed that agreement of the GENIE calculations with data is satisfactory. But, we found that the GENIE models as well as the RDWIA should be enriched with additional effects that are not directly related to the single-nucleon knockout. So, the direct comparison of spectral functions, implemented in neutrino event generators, with the precise electron reduced cross section data presents a great opportunity to test better the accuracy of the nuclear effect calculations.

ACKNOWLEDGMENTS

The author greatly acknowledge A. Habig for fruitful discussions and a critical reading of the manuscript.

-
- [1] M. A. Acero *et al.*, (NOvA Collaboration), Phys. Rev. Lett. **123**, 151803 (2019).
 - [2] K. Abe *et al.*, (T2K Collaboration), Phys. Rev. Lett. **121**, 171802 (2018).
 - [3] R. Acciarri *et al.*, (DUNE Collaboration), FERMILAB-DESIGN-2016-03.
 - [4] K. Abe *et al.*, (Hyper-Kamiokande Collaboration) arXiv:1805.04163 [physics.ins-det].
 - [5] M. Antonello *et al.* (MicroBooNE, LAr1-ND, ICARUS-WA104 Collaboration), arXiv:1503.01520 [physics.ins-det].
 - [6] A. Picklesimer, J. W. Van Orden, S. J. Wallace, Phys. Rev. **C 32**, 1312 (1985).
 - [7] J. M. Udias, P. Sarriguren, E. Moya de Guerra, E. Garrido, and J. A. Caballero, Phys. Rev. **C 51**, 3246 (1995).
 - [8] James J. Kelly, Phys. Rev. **C 59**, 3256 (1999).
 - [9] R. Gonzalez-Jimenez, M. B. Barbaro, J. A. Caballero, T. W. Donnelly, N. Jachowicz, G. D. Megias, K. Niewczas, A. Nikolakopoulos, J. M. Udias, Phys. Rev. **C 101**, 015503 (2020).
 - [10] A. V. Butkevich and S. V. Luchuk, Phys. Rev. **C 102** 024602 (2020).
 - [11] G. D. Megias, J. E. Amaro, M. B. Barbaro, J. A. Caballero, T. W. Donnelly, Phys. Rev. **D 94**, 013012 (2016).
 - [12] G. D. Megias, J. E. Amaro, M. B. Barbaro, J. A. Caballero, T. W. Donnelly, and I. R. Simo, Phys. Rev. **D 94**, 093004 (2016).
 - [13] A. M. Ankowski and A. Friedland, Phys. Rev. **D 102**, 053001 (2020).
 - [14] A. Papadopoulou *et al.* (e4v Collaboration) Phys. Rev. **D 103**, 113003 (2021).
 - [15] M. Khachatryan, A. Papadopoulou, A. Ashkenazi, F. Hauenstein, L. B. Weinstein, O. Hen, E. Piasetzky (CLAS and e4v Collaboration), Nature **599**, 565 (2021).
 - [16] L. Alvarez-Ruso, *et al.* (GENIE Collaboration), Eur. Phys. J. Spec. Top. **230**, 4449 (2021).
 - [17] J. Zmuda, K. Graczyk, C. Juszczak, and J. Sobczyk, Acta. Phys. Pol. B46, 2329 (2015).

- [18] R. D. Banerjee, A. M. Ankowski, K. M. Graczyk, B. E. Kowal, H. Prasad, and J. T. Sobczyk, Phys. Rev. **D 109**, 073004 (2024).
- [19] J. Isaacson, W. J. Jay, A. Lovato, P. A. N. Machado, and N. Rocco, Phys. Rev. **D 107**, 033007 (2023).
- [20] S. Abe, Phys. Rev. **D 111**, 033006 (2025).
- [21] S. Dytman, Y. Hayato, R. Raboanary, J. T. Sobczyk, J. Tena Vidal and N. Vololoniaina, Phys. Rev. **D 104**, 053006 (2021).
- [22] K. Niewczas, and J. T. Sobczyk, Phys. Rev. **C 100**, 015505 (2019).
- [23] A. V. Butkevich and S. A. Kulagin, Phys. Rev. **C 76**, 045502 (2007).
- [24] A. V. Butkevich, Phys. Rev. **C 80**, 014610 (2009).
- [25] A. V. Butkevich, Phys. Rev. **C 85**, 065501 (2012).
- [26] A. V. Butkevich, Phys. Rev. **C 109**, 045502 (2024).
- [27] C. Andreopoulos, A. Bell, D. Bhattacharya, F. Cavanna, J. Dobson, S. Dytman, H. Gallagher, P. Guzowski, R. Hatcher, P. Kehayias *et al*, Nucl. Instrum. Meth. **A614**, 87 (2010).
- [28] The GENIE Event Generator, <http://genie-mc.org>
- [29] J. A. Caballero, T. W. Donnelly, E. Moya de Guerra, and J. M. Udias, Nucl. Phys. **A 632**, 323 (1998).
- [30] A. Nikolakopoulos, R. Gonzalez-Jimenez, N. Jachowicz, K. Niewczas, F. Sanchez, J. M. Udias, Phys. Rev. **C 105** 054603 (2022).
- [31] K. Nakamura, and N. Izutsu, Nucl. Phys. **A 259**, 301 (1976).
- [32] J. J. Kelly, Phys. Rev. **C 71**, 064610 (2005).
- [33] J. Mougey, M. Bernheim, A. Bussiere, A. Gillebert, P. X. Ho, M. Priou, D. Royer, I. Sick, and G. Wagner, Nucl. Phys. **A 262**, 461 (1976).
- [34] N. C. R. Makins, R. Ent, M. S. Chapman, J. O. Hansen, K. Lee, Milner R.G. *et al.*, Phys. Rev. Lett. **72**, 1986 (1994).
- [35] D. Dutta *et al.*, Phys. Rev. **C 68**, 064603 (2003).
- [36] C. Andreopoulos, C. Barry, S. Dytman, H. Gallagher, T. Golan, R. Hatcher, G. Perdue, J. Yarba, arXiv:1510.05494.
- [37] L. Alvarez-Russo *et al.*, (GENIE Collaboration), Eur. Phys. J. Spec. Top. **230**, 4449 (2021).
- [38] J. Tena-Vidal *et al.*, (GENIE Collaboration), Phys. Rev. **D 106**, 112001 (2022).

- [39] S. J. Mashnik, A. J. Sierk, K. K. Gudima, and M. I. Baznat, J. Phys. Conf. Ser. **41**, 340 (2006).
- [40] A. Bodek and J. L. Ritchie, Phys. Rev. **D 23**, 1070 (1981).
- [41] C. Llewellyn Smith, Phys. Rep. **3**, 261 (1972).
- [42] J. Nieves, I. Ruiz Simo, and M. J. Vicente Vacas, Phys. Lett. **B 707**, 72 (2012).
- [43] J. Nieves, J. E. Amaro, and M. Valverde, Phys. Rev. **C 70**, 055503 (2004). Phys. Rev. D106, 112001 (2022)
- [44] R. Gran, J. Nieves, F. Sanchez, and M. J. Vicente Vacas, Phys. Rev. **D88**, 113007 (2013).
- [45] S. Dolan, G. D. Megias, and S. Bolognesi, Phys. Rev. **C 101**, 033003 (2020).
- [46] O. Benhar, A. Fabrocini, S. Fantoni, Nucl. Phys. **A 505**, 267 (1989).
- [47] O. Benhar, A. Fabrocini, S. Fantoni, Nucl. Phys. **A 579**, 493 (1994).
- [48] A. Bodek, H. S. Budd, M. E. Christy, Eur. Phys. J. **C 71**, 1726 (2011).
- [49] A. Bodek, H. S. Budd, M. E. Christy, B. Coopersmith, Eur. Phys. J. **C 74**, 3091 (2014).
- [50] J. McKean, R. Gonzalez-Jimenez, M. Kabirnezhad, J. M. Udias, arXiv:2502.10629
- [51] G. Garino, *et al.*, Phys. Rev. **C 45**, 780 (1992).
- [52] D. Rohe *et al.*, Phys. Rev. **C 72**, 054602 (2005).